



ELSEVIER

Contents lists available at ScienceDirect

## Journal of Magnetism and Magnetic Materials

journal homepage: [www.elsevier.com/locate/jmmm](http://www.elsevier.com/locate/jmmm)

## Research articles

Giant hydrogen effect on the structure and physical properties of ZnO and Co-doped ZnO films fabricated by the RF magnetron sputtering in Ar + H<sub>2</sub> atmosphereI.S. Edelman<sup>a</sup>, Hsiung Chou<sup>b,c</sup>, Yu.E. Samoshkina<sup>a,\*</sup>, D.A. Petrov<sup>a</sup>, Hsien C. Lin<sup>b</sup>, Wen L. Chan<sup>b</sup>, Shih-Jye Sun<sup>b</sup>, S.M. Zharkov<sup>a,d</sup>, G.V. Bondarenko<sup>a</sup>, M.S. Platonov<sup>a,e</sup>, A. Rogalev<sup>e</sup><sup>a</sup> Kirensky Institute of Physics, Federal Research Center KSC SB RAS, 660036 Krasnoyarsk, Russia<sup>b</sup> Department of Physics, National Sun Yat-sen University, 80424 Kaohsiung, Taiwan, ROC<sup>c</sup> Department of Applied Physics, National University of Kaohsiung, 81148 Kaohsiung, Taiwan, ROC<sup>d</sup> Siberian Federal University, 660041 Krasnoyarsk, Russia<sup>e</sup> European Synchrotron Radiation Facility (ESRF), CS 40220, 38043 Grenoble Cedex, France

## ARTICLE INFO

## Keywords:

ZnO films  
Co-doped ZnO films  
Films hydrogenation  
Magnetic circular dichroism  
Room temperature ferromagnetism

## ABSTRACT

ZnO and Co-doped ZnO films were synthesized by the radio frequency magnetron sputtering in mixed atmosphere of Ar + 20% O<sub>2</sub> and Ar + 20–50% H<sub>2</sub>. The morphology, chemical composition, crystal structure, optical transmission, electrical resistance, and magnetic circular dichroism of the films were investigated. It was established that the films thickness decreased several times when Ar was partly replaced by hydrogen in the sputtering chamber. At the same time, for the Co-doped ZnO films, the increase in the relative Co content with the increasing hydrogen concentration was observed. These phenomena are explained by the formation of gaseous ZnH<sub>2</sub> because of the hydrogen reaction with the growing films under the conditions of the high substrate temperature (450 °C) and, respectively, the decrease in the Zn component in the films. The hydrogenated Co-doped ZnO films exhibit an increase in electric conductivity and ferromagnetic behavior at room temperature. The magnetic nature of the films is explained by a combination of the intrinsic ferromagnetism (due to the formation of the Co-H-Co complex) with the inclusion of metallic Co clusters.

## 1. Introduction

Diluted magnetic semiconductors (DMS) are currently at the focus of attention of researchers and new technology developers due to their extraordinary properties such as a combination of the semiconductor conductivity type with ferromagnetism, high magneto-caloric effects, optical properties depending on the magnetic state, large magnetoresistance, etc. In particular, they are promising materials for spintronic devices [1–3]. Potentially, DMS are cost-effective alternatives to provide the up-scale front contacts for thin film solar cells [4]. ZnO films doped with transition ions belong to this class of materials. Special attention is paid to Co-doped ZnO films due to possible room temperature ferromagnetism with a low content of cobalt in the samples. However, it has been established that the appearance of ferromagnetism in such materials depends critically on the conditions of fabrication and post-fabrication treatment of the samples. A detailed review of different methods used for the fabrication of ZnO and Co-

doped ZnO films was presented in [5]. Pulsed laser deposition [6], metal–organic chemical vapor deposition [7], molecular beam epitaxy [8,9], and radio frequency (RF) magnetron sputtering [10–12] are among the most commonly used methods of the films fabrication. Some authors used sol–gel dip coating process [13]. Sol-gel methods were also used to fabricate a Co-doped ZnO powder [14–16].

Many authors used hydrogenation as an effective method to improve magnetic and transport properties of ZnO and Co-doped ZnO samples. The first experiments on the effect of hydrogen on the ZnO conductivity date back to the 1950-ties: hydrogen was introduced into a ZnO single crystal under pressure at high temperature and caused an increase in its conductivity [17]. The same method was used in Refs. [14–16] in order to induce ferromagnetism in the Co-doped ZnO samples. The method of post-annealing in the hydrogen H<sub>2</sub> gas atmosphere was also used in [18,19]. The magnetic properties of Co (10%)-doped ZnO nano-crystalline powder fabricated with the sol–gel method were studied in Ref. [14]. An appearance of the room temperature

\* Corresponding author.

E-mail address: [uliyag@iph.krasn.ru](mailto:uliyag@iph.krasn.ru) (Y.E. Samoshkina).<https://doi.org/10.1016/j.jmmm.2019.165461>

Received 11 March 2019; Received in revised form 14 May 2019; Accepted 13 June 2019

Available online 14 June 2019

0304-8853/ © 2019 Elsevier B.V. All rights reserved.

ferromagnetism in the powder after its hydrogen plasma treatment was shown. Such behavior was explained by the short-range spin ordering due to the formation of a Co-H-Co complexes. The Co (15%)- and Co (20%)-doped ZnO powders fabricated by the sol-gel methods were investigated in Ref. [15]. The samples also showed ferromagnetism at room temperature after hydrogen injection performed by plasma treatment with Ar-H<sub>2</sub> mixed gas. For the Co (15%)-doped ZnO sample, the enlarged magnetization was attributed to the contribution of Co-H-Co spin units, while the ferromagnetism of the Co (20%)-doped ZnO powder was explained by the contribution of both the Co-H-Co spin units and metallic Co phase. It should be noted that, in the works known to us, the hydrogen concentration in the mixed gas during treatment of the samples was up to 15%.

Only several works are available in literature devoted to the Co-doped ZnO films synthesized using the RF magnetron sputtering in an Ar-H<sub>2</sub> mixed gas environment [10,11]. The ZnO films with the cobalt content of 5–10% were prepared at the hydrogen content in the sputtering chamber up to 5%. The deposited films demonstrated ferromagnetism almost up to the room temperature. These works gave impetus to the further development of the methodology of the films magnetron sputtering in an atmosphere enriched with hydrogen, and the study physical properties of the films prepared with this technology.

With the aim to enhance the magnetic response of the ZnO and Co-doped ZnO films, we fabricated these samples by the RF magnetron sputtering at higher hydrogen concentration in the sputtering chamber (from 20 to 50%.) For comparison, the same films were prepared in Ar + 20% O<sub>2</sub> atmosphere. The process parameters used led to unexpected results. With the growth of H<sub>2</sub> concentration in a chamber the strong change in the Zn:Co ratio was revealed in the sample comparing to that in the sputtered target. Such phenomenon (revealed here for the first time) affect the physical properties of the films. In the paper, we present a detailed study of the morphology, crystal structure, chemical composition, magnetic, optical and electrical properties of the ZnO and Co-doped ZnO films in relation to the H<sub>2</sub> concentration during the deposition process.

## 2. Material and methods

### 2.1. Samples synthesis

The films were grown on a glass substrate by the standard RF magnetron sputtering system using the two inches ZnO (ZO) and Zn<sub>0.95</sub>Co<sub>0.05</sub>O (CZO) targets. The targets were synthesized from the high purity ZnO (99.999%) powder or the ZnO (99.999%) and Co<sub>3</sub>O<sub>4</sub> (99.9985%) powders by a solid state reaction process with several intermediate grindings. The ZO and CZO targets were calcined at 1300 °C for 12 h in atmosphere of flowing oxygen and 860 °C for 12 h in atmosphere of flowing argon gas. The films were deposited at a total pressure of 30 mTorr and a forward RF power of 80 W at the substrate temperature 450 °C for 20 min. Five samples of each composition were prepared with the following mixed gas in the chamber: Ar + 20% O<sub>2</sub>, Ar + (20%, 30%, 40%, 50%) H<sub>2</sub>, samples ZO1, ZO2, ZO3, ZO4, ZO5, and CZO1, CZO2, CZO3, CZO4, CZO5, respectively.

### 2.2. Methods

The films morphology was determined using the high-resolution transmission electron microscope (HRTEM) JEOL JEM-2100 (LaB<sub>6</sub>) with the accelerating voltage 200 kV, equipped with the energy dispersive X-ray spectrometer Oxford Inca x-sight, and a complex for sample preparation including focused ion beam (FIB). Selected-area electron diffraction (SAED) and the grazing incidence angle X-ray diffraction (GIXRD) were used to determine the crystal structure of the films. The films composition was examined with X-ray fluorescent analysis (XRFA) using a spectrometer S4 PIONEER (Bruker). For two samples, CZO2 and CZO3, the XANES (X-ray absorption near edge

structure) spectra were measured at the Co K- absorption edge (7709 eV). Measurements were performed at the European Synchrotron Radiation Facility (ESRF), the ID12 beamline, using total fluorescence yield detection mode in back-scattering geometry [20].

The electrical resistivity of the films was investigated at room temperature using the standard four-point probe technique. The optical transmittance was measured at room temperature with an N&K spectrometer.

The magnetic properties of the samples were studied by magnetic circular dichroism (MCD) at the optical frequencies. MCD, on the one hand, provides information on electronic transitions from the ground to the excited states of magnetic ions. On the other hand, MCD reflects the magnetic behavior of the sample, since this effect is linear in the magnetic field. MCD was measured in the normal geometry: the magnetic vector and the light beam were directed normal to the films plane. The modulation of the polarization state of the light wave from the right-hand to the left-hand circular polarization relatively to the magnetic field direction was used. The MCD value was measured by the formula  $\Delta k = (D_+ - D_-)/d$ , where  $D_+$  and  $D_-$  are the optical density of the films for right and left polarized waves, and  $d$  is the films thickness. Measurements were carried out in the spectral range 1.2–4.5 eV in a magnetic field up to 13 kOe at the temperature 300 K. The measurement accuracy was about  $10^{-4}$ , and the spectral resolution was  $20\text{--}50\text{ cm}^{-1}$  depending on the wavelength.

## 3. Results

### 3.1. Morphology, structure, and chemical composition

XRFA data for both series of the films are collected in Tables 1 and 2. The thickness of the ZO1 and CZO1 films is large enough (~160 nm) and practically the same for both samples. The composition of the CZO1 film corresponds to the target composition. The substitution of oxygen for hydrogen in the sputtering chamber leads to the dramatic change of the film characteristics. The film thickness decreases almost by an order of magnitude for the ZO2 film and more than twice for the CZO2 film compared to the ZO1 and CZO1 samples, respectively. A further increase in the hydrogen concentration in the sputtering chamber causes a smoother decrease in the film thickness up to 14 nm for the ZO5 film and 31.6 nm for the CZO5 film. The thickness decrease in the CZO series is accompanied by increase in the Co content relative to the Zn content in the films from 0.05 for CZO1 to 0.39 for CZO5. Examples of the cross-sections HRTEM image for the samples from the ZO and CZO series are shown in Figs. 1a and 2. A comparison of Figs. 1a and 2 confirms the abrupt decrease in the film thickness at the transition from Ar + 20% O<sub>2</sub> atmosphere (Fig. 1a) to Ar + 30% H<sub>2</sub> and Ar + 50% H<sub>2</sub> (Fig. 2). Some discrepancy in the thickness of the ZO and CZO films is seen between the results obtained with XRFA and HRTEM. This is because the FIB technique of the sample preparation can destroy a part of the surface, making the film thinner. Nevertheless, the XRFA and HRTEM data correlate well.

SAED patterns for the ZO1 film (Fig. 1b) demonstrate an almost ideal wurtzite crystal structure of the samples. For the CZO films, the GIXRD patterns are presented in Fig. 3. The diffraction peaks, as well, correspond to the ZnO lattice with a hexagonal wurtzite crystal structure P63mc. The most intense diffraction peaks observed in Figs. 1b and

**Table 1**  
The XRFA and resistivity data for the ZnO films.

Sample	Film thickness, nm	Resistivity, Ohm* $\mu$ m
ZO1	167	Over 25
ZO2	20.5	Over 3.2
ZO3	16.5	Over 2.3
ZO4	15.5	Over 2.3
ZO5	14	Over 2.3

**Table 2**

The XRFA and resistivity data for the Co-doped ZnO films.  $Co_x$  is the relative Co content in the film.

Sample	$Co_x$	Film thickness, nm	Resistivity, $\Omega \cdot m$
CZO1	0.052	159.9	Over 22.7
CZO2	0.234	71.7	$11.8 \cdot 10^{-4}$
CZO3	0.279	53.5	$63.5 \cdot 10^{-5}$
CZO4	0.346	37	$15.9 \cdot 10^{-5}$
CZO5	0.390	31.6	$14.5 \cdot 10^{-5}$

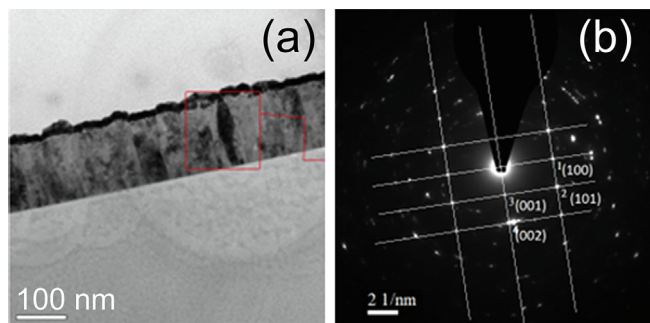


Fig. 1. Cross-section HRTEM image (a) and SAED pattern (b) for the ZO1 sample.

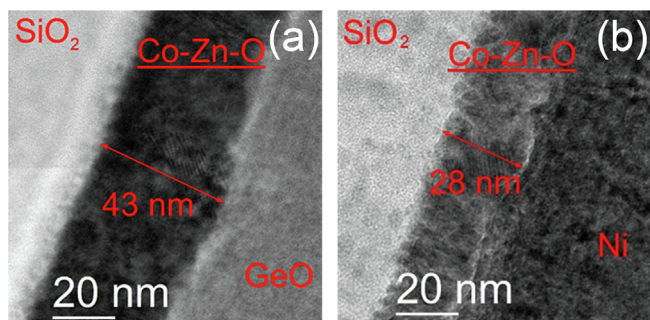


Fig. 2. Cross-section HRTEM images for the CZO3 (a) and CZO5 (b) samples.

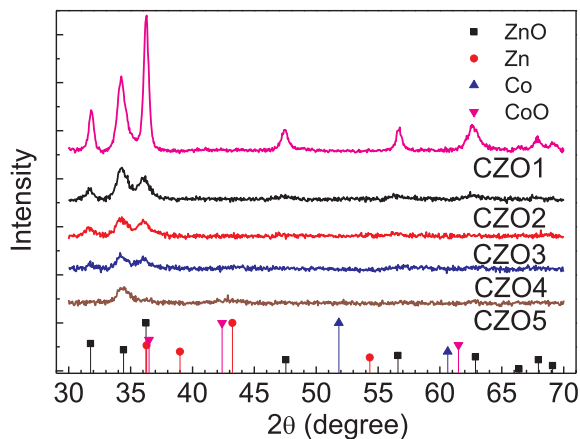


Fig. 3. GIXRD patterns for the CZO samples.

3 correspond to (1 0 0), (0 0 2), and (1 0 1) planes of ZnO and indicate the polycrystalline structure of the films. It should be noted that, when  $O_2$  is replaced by  $H_2$  in the sputtering chamber, all the peak intensity decreases sharply, and the peak intensity in the region  $2\theta$  from 30 to 37 degrees redistributes (Fig. 3). Such a behavior indicates the decrease in the crystallite size in the samples and a change in their preferable orientations with the increasing hydrogen concentration. Thus, the

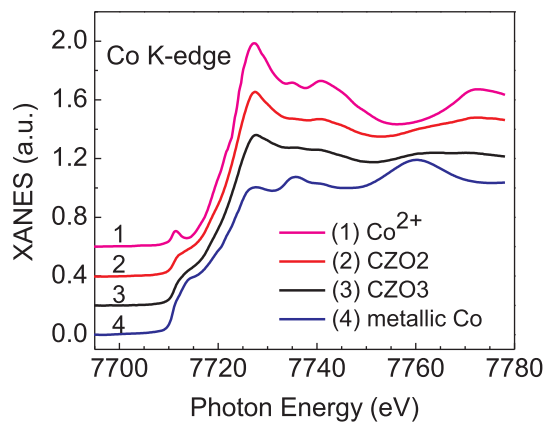


Fig. 4. Experimental XANES spectra at the Co K-edge for the Co-doped ZnO samples together with the reference XANES spectra of metallic Co and  $Co^{2+}$  in ZnO taken from Ref. [21].

introduction of hydrogen into the sputtering chamber does not only reduce the amount of the deposited ZnO, but it also affects the film crystal structure. Taking into account the increase in the relative Co content in the CZO samples with the increase in the  $H_2$  concentration (Table 2), one could expect the formation of secondary Co phases. However, no other crystal phases associated with Co are observed in the GIXRD patterns.

To get an insight on the electronic configuration of Co in the samples, we used the XANES spectroscopy at the Co K-edge. This technique is known to be an element-selective and highly sensitive tool to study local electronic structure of absorbing atoms. The experimental XANES spectra for two Co-doped ZnO samples together with the reference XANES spectra for metallic Co and  $Co^{2+}$  in ZnO [3,21] are shown in Fig. 4. As one can see from Fig. 4, the XANES spectra for both films indicate a mixed state of Co in the samples.

We tried to estimate the amount of  $Co^{2+}$  and metallic Co in these samples. The experimental XANES spectra were compared with the weighted sums of the reference XANES spectra of the metallic Co and  $Co^{2+}$  in ZnO [3,21]. The results of this comparison are shown in Fig. 5. A very good agreement was found with 40% of cobalt in the metallic state and 60% of  $Co^{2+}$  ions for the CZO2 sample, and 60% of metallic cobalt and only 40% of  $Co^{2+}$  ions for the CZO3 film. These results unambiguously confirm the presence of metallic Co clusters in both films. At the same time, the amount of metallic Co clusters increases by 50% at the transition from the CZO2 sample to the CZO3 one, that is, with the increase in the hydrogen concentration during the deposition process of the films.

### 3.2. Optical, electrical and magneto-optical properties

Changes in the morphology and chemical composition of the films caused by the hydrogen addition into the sputtering chamber are accompanied by changes in their physical properties. The optical transmittance spectra for all the samples are presented in Fig. 6. All ZO and CZO1 films have about 90% transparency in the visible region, while in the hydrogenated CZO films the transparency is lower and decreases from 55 to 35% with increasing  $H_2$ . Besides, at the transition from  $Ar + O_2$  to  $Ar + H_2$  atmosphere the absorption edge of the films shifts to the higher energy region.

The optical absorption ( $\alpha$ ) spectra and the band gap ( $E_g$ ) for the studied films were calculated from the transmittance spectra in the strong absorption region, where reflection can be neglected. Using the Beer-Lambert law (1), and then the Tauc model (2),  $E_g$  was estimated by assuming a direct transition between the valence and conduction bands. For the samples deposited in  $Ar + O_2$  atmosphere,  $E_g$  was found to be  $\approx 3.3$  eV that is close to 3.31 eV for bulk ZnO [22] and 3.26 eV for ZnO

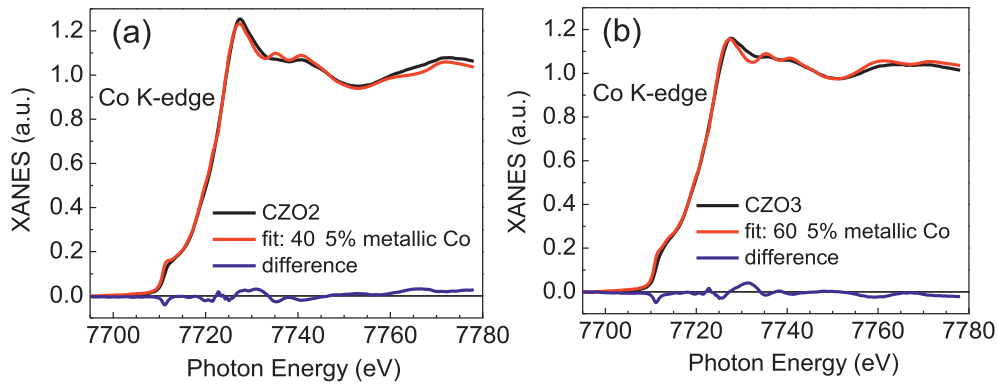


Fig. 5. Comparison of the experimental XANES spectra at the Co K-edge for the CZO2 (a) and CZO3 (b) samples with the weighted sums of the reference spectra of metallic Co and  $\text{Co}^{2+}$  in ZnO.

micro-rods [23]. For the hydrogenated ZO and CZO samples,  $E_g \approx 4.6$  eV and 4.5 eV, respectively. Inside each ZO and CZO series  $E_g$  changes insignificantly when the  $\text{H}_2$  concentration changes in the sputtering chamber. Thus, the high hydrogenation of the ZO and CZO films leads to an increase in the band gap in the samples.

$$\alpha = (1/d) \ln(1/T) \quad (1)$$

where  $d$  and  $T$  are the film thickness and transmittance value, respectively.

$$(\alpha h\nu)^2 = A(h\nu - E_g) \quad (2)$$

where  $h\nu$  is the energy of the incident photon, and  $A$  is the energy-independent constant.

Ordinarily, materials with a band gap width more than 4 eV are referred to as dielectrics. However, the electrical resistivity of the CZO2-CZO5 films indicates their semiconductor nature. As it is seen from Tables 1 and 2, the electric resistivity is higher than  $2.3 \text{ Ohm}\cdot\text{m}$  for all the ZO samples and for the CZO sample deposited in  $\text{Ar} + \text{O}_2$  atmosphere, which is typical for dielectrics. Herewith, the resistivity value decreases by 4–5 orders for the CZO films deposited in  $\text{Ar} + \text{H}_2$  atmosphere and depends on the hydrogen concentration. Such a behavior reflects an enhancement in the electrical conductivity of the films with the increasing  $\text{H}_2$  concentration.

MCD spectra for ZO2, ZO5 and all CZO films are shown in Fig. 7 and 8a, respectively. For the ZO1 sample, there was no MCD signal within the accuracy of the experiment. Such a behavior is consistent with the MCD data presented for the ZnO in Ref. [24]. For the ZO2-ZO5 films, the MCD spectra represent a wide negative peak centered near the ZnO band edge. The intensity of this peak grows with the increase in the hydrogen concentration during the deposition process of the films (example in Fig. 7). The MCD value in this region is approximately linear on the magnetic field up to highest magnetic field

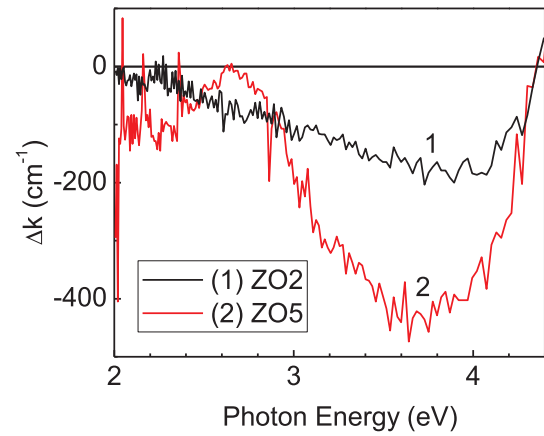


Fig. 7. MCD spectra for the ZO2 and ZO5 films at  $T = 300$  K in the magnetic field  $H = 13$  kOe.

used, 13 kOe (not shown). Too high noise does not allow one to judge about the low energy part of the spectra.

For the CZO1 film, the extremely weak feature of the s-shape near 2 eV, as well as a very weak but wide positive peak centered at 3.4 eV are seen (Insert in Fig. 8a). Similar to the ZO samples, the MCD value for this film near 3.4 eV is linear on the magnetic field (not shown). Note that the MCD dependence on magnetic field for the CZO1 sample is the same in the whole investigated spectral range. The hydrogen addition during the deposition of the CZO films leads to strong changes in the MCD spectra, namely the intense signals of different signs appear (curve 2 in Fig. 8a). The further increase in the  $\text{H}_2$  concentration causes a rearrangement of the MCD spectrum for the CZO3-CZO5 films (curves 3–5 in Fig. 8a).

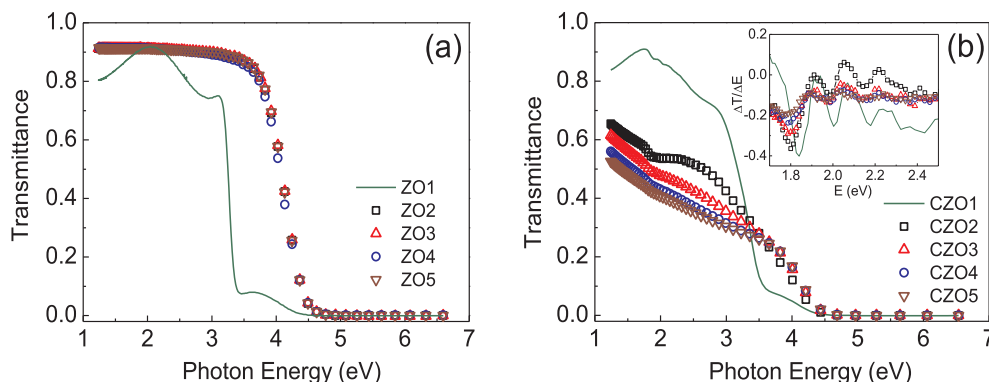
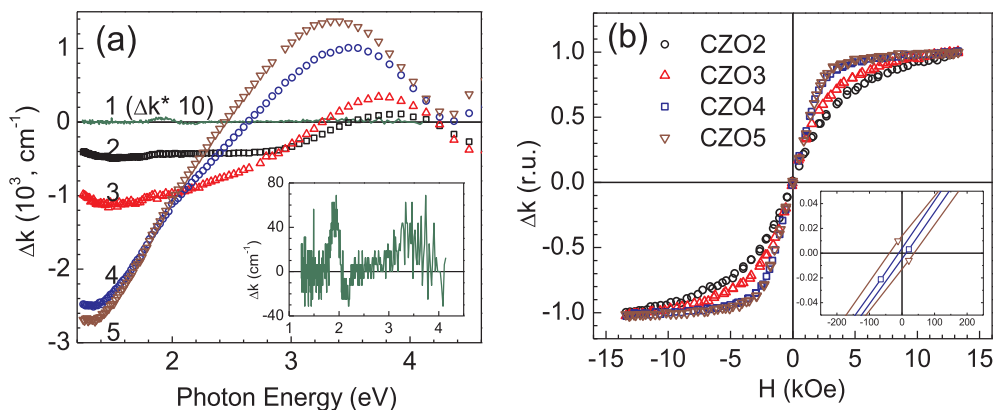


Fig. 6. Optical transmittance ( $T$ ) spectra for the ZO (a) and CZO (b) films. Insert:  $dT/dE$  in the region 1.7–2.5 eV for the CZO films.



**Fig. 8.** a – MCD spectra for the CZO1-CZO5 samples, curves 1–5, respectively.  $H = 13$  kOe,  $T = 300$  K. Insert: the magnified MCD spectrum for CZO1; b – MCD hysteresis loops for the CZO2-CZO5 samples.  $E = 1.55$  eV,  $T = 300$  K. Insert: low field parts of the MCD hysteresis loops for the CZO4 and CZO5 samples.

For all the CZO2-CZO5 films, the MCD dependence on external magnetic field is described by a hysteresis loop as it is seen from Fig. 8b. Herewith, the hysteresis loops for the CZO4 and CZO5 samples are more rectangular with the saturation field ( $H_s$ ) near 5 kOe. The coercivity for the CZO2-CZO5 samples is about 10–40 Oe (Insert in Fig. 8b). The field MCD dependence is the same in the whole investigated spectral range.

#### 4. Discussion

An extremely strong effect of hydrogen on the morphology, composition, and structure of the samples can be explained by the fact that  $H_2$  reacts with the ZnO and Co-doped ZnO layers formed on the glass substrate heated to 450 °C. Earlier, it was thought, that Zn did not react with  $H_2$ . However, since 1987 studies appeared indicating the possibility of this reaction resulting in the fabrication of  $ZnH_2$  both in the solid [25,26] and gaseous state [27]. Shayesteh with co-authors synthesized gaseous  $ZnH_2$  [27], they placed a zinc rod into an alumina tube and heated it to 470 °C. Pure hydrogen floated slowly through the tube, the DC discharge (3 kV, 333 mA) was applied between two electrodes located inside the water-cooled ends of the alumina tube. The  $ZnH_2$  gas was detected directly in the tube with the help of infrared spectroscopy through the special windows in the tube. Our experimental conditions (the substrate temperature 450 °C and  $H_2$  migrating between the target and substrate) are close to those used in Ref. [27]. Therefore, the reaction (3) with the formation of gaseous  $ZnH_2$  seems to be possible. Such a reaction can explain the decrease in the film thickness and redistribution of Co and Zn contents in the samples.



The MCD spectrum for the CZO1 sample is similar to that for the Co-doped ZnO materials with the low Co content observed by other authors [24,28–33]. The MCD spectrum for the CZO1 sample is particularly close to the room temperature MCD spectrum for the Co (9.3%) – doped ZnO film grown on a glass substrate by magnetron sputtering in Ar atmosphere [33]. The authors of the cited articles assigned the MCD features near 2 eV (namely 1.8, 2, and 2.2 eV) to the d-d transitions of the  $Co^{2+}$  ions in the  $T_d$  symmetry sites. Similar features were observed both in the optical and magneto-optical spectra, and it was indicated that the Co ions substituted Zn in the wurtzite ZnO lattice [28–31,34,35]. The features near 2 eV were also observed in the optical transmittance spectra for all the CZO films. The weak peaks are well visible in the transmittance derivative  $dT/dE$  spectra (Insert in Fig. 6b). At first sight, the decrease in the intensity of the  $dT/dE$  peaks for the samples deposited at the 30–50%  $H_2$  concentration seems to be strange, taking into account the increasing relative Co content in the films. However, it should be remembered that the relative Co content only increases due to the decrease in the Zn content. On the other hand, the possible changes in the Co valence state and structural disorder of the

film can reduce the contribution of the d-d transitions in  $Co^{2+}$  ions into optical transmission spectrum. The feature of the MCD spectrum near 3.5 eV was assigned to the ZnO band edge [26,30,32]. It should be noted that in all the specified works the MCD signal in the Co-doped ZnO samples demonstrated the linear dependence on the external magnetic field.

The MCD spectrum for the CZO2 sample is in good agreement with that for the Co-doped ZnO films (with 19% and 20% of Co) grown on sapphire (0 0 1) substrates by magnetron sputtering in Ar atmosphere [35]. The strong positive peak in the region 3.5–3.9 eV shifting to lower energy with an increase in the relative Co content, the strong negative peaks near 1.5 and 2.6 eV, and the small fluctuations near 2 eV observed in our case coincide practically with the analogous features presented in Ref. [35]. Herewith, the field MCD dependences for the Co-doped ZnO films (with 19% and 20% of Co) exhibited clear ferromagnetic behavior. Such a behavior was explained by the presence of Co clusters in the samples.

As it was mentioned in the introduction, various research groups observed noticeable improvement of the magnetic properties of Co-doped ZnO samples by the addition of  $H_2$  in both the production and the treatment processes. This behavior was explained by either spin–spin interaction induced by hydrogen mediation (due to the formation of the Co-H-Co complex), for example, Refs. [12,15], or H-induced formation of cobalt oxide phases and their subsequent reduction to metallic Co clusters [10,15,34]. The formation of Co oxides in the fabrication process of Co (10%) – doped ZnO powders was considered in Ref. [36] in more detail. In the specified work the precise conditions required to fabricate samples with the intrinsic ferromagnetism and the ferromagnetism caused by the existence of secondary Co oxide phases were identified. The authors confirmed that the treatment temperature above 300 K lead to a greater amount of  $Co_3O_4$  in the Co-doped ZnO powder without visible ferromagnetism. Further hydrogen treatment of the samples by hot isostatic pressing transformed  $Co_3O_4$  into metallic Co clusters, which directly contributed to ferromagnetism. Some authors reported on formation of metal clusters in the ZnO films doped with other transition metals, such as nickel [37].

Comparing the results obtained in the present study with the results available in literature and analysis data of the XANES spectra (Fig. 5), we can state in the investigated films a complex nature of magnetism assuming a combination of the intrinsic ferromagnetism (due to the formation of the Co-H-Co complex) with the ferromagnetic inclusions, namely metallic Co clusters. Taking into account the relatively high Co content in the CZO2-CZO5 films, one can assume that the MCD signal is conditioned, at least partly, by the presence of Co clusters in the samples. Such clusters in the CZO2-CZO5 films could arise under the sputtering conditions used (Ar +  $H_2$  atmosphere and substrate temperature of 450 °C) in accordance with reaction (4).



Besides, the MCD spectra and MCD field dependencies for the CZO2-CZO5 films under study can be compared with those for Co particles ion-synthesized in the amorphous matrix of silicon dioxide [38,39]. The changes in the magnetic response of such samples were traced at room temperature with an increase in the Co particles size as successive transitions of the paramagnetic-superparamagnetic-ferromagnetic state. A rearrangement of the MCD spectrum with the particle size increase was observed in the range of 1.5–3.0 eV, namely a shift of the spectral weight to low-energy region and the MCD signal increase (Fig. 3b in Ref. [39]). The MCD spectral behavior observed for CZO2-CZO5 films in the range of 1.2–3.0 eV is close to the MCD behavior of the Co implanted samples mentioned above.

## 5. Conclusions

ZnO and Co-doped ZnO films were synthesized by the RF magnetron sputtering of ZnO and Zn<sub>0.95</sub>Co<sub>0.05</sub>O targets in mixed Ar + 20% O<sub>2</sub> and Ar + 20–50% H<sub>2</sub> atmosphere onto glass substrates heated to 450 °C. It is established that, in the case of the ZnO films, the presence of hydrogen in the sputtering chamber strongly affects the morphology, crystal structure, and optical properties of the samples. The films thickness decreases when oxygen is replaced by hydrogen in the sputtering chamber and continues to decrease as the hydrogen concentration increases. In addition, with the increasing hydrogen, the crystallite size in the samples decreases and their orientations become random. The fundamental absorption edge shifts to the high-energy region, the width of the optical band gap increases and becomes equal to 4.6 eV. The value of the optical transparency does not change meanwhile and is equal 90%. The MCD data indicate the paramagnetic state of all the ZnO films with the electric resistivity over 2.3 Ohm\*cm.

In the case of the Co-doped ZnO films, the presence of hydrogen in the sputtering chamber strongly affects not only the morphology, crystal structure, and optical properties of the samples, similarly to the ZnO films, but also their chemical composition, electric resistivity value, and magnetic properties. The relative Co content increases from 5% in the film deposited in Ar + 20% O<sub>2</sub> atmosphere to 39% in the film deposited in Ar + 50% H<sub>2</sub> atmosphere. Thus, the decrease in the total thickness of the films is due to the decrease in the Zn content. The electric conductivity of the films increases with the increasing H<sub>2</sub> concentration. Unlike the Co-doped ZnO films synthesized in atmosphere Ar + O<sub>2</sub>, the hydrogenated Co-doped ZnO films exhibit ferromagnetic behavior at room temperature. However, the optical transparency of the samples decreases from 80 to 35%.

We suppose that a combination of the high hydrogen concentration in the sputtering chamber and high temperature of the substrate provides conditions for a chemical reaction of H<sub>2</sub> with the growing ZnO film. As a result of this reaction, gaseous ZnH<sub>2</sub> and water are formed and the Zn content in the films decreases. The reaction intensity increases with the increasing H<sub>2</sub> concentration in the sputtering chamber that leads to further reduction of the Zn content in the films. Since X-ray absorption spectroscopy unambiguously revealed the presence of metallic Co clusters in the samples, we considered the formation of metallic Co clusters as one of possible mechanisms of the ferromagnetic behavior of CZO2-CZO5 samples. The clusters are the products of the formation of Co<sub>3</sub>O<sub>4</sub> and then its reduction to the metallic state. Thus, the hydrogen concentration and substrate temperature turned out to be critical for the growth processes of the ZnO and Co-doped ZnO films.

## Acknowledgements

The work is supported by the Russian Academy of Sciences in the frames of Project № 0356-2017-0030 and by the Ministry of Science and Technology of Taiwan MOST 106-2112-M-110-001.

## References

- [1] A. Ney, V. Ney, S. Ye, K. Ollefs, T. Kammermeier, T.C. Kaspar, S.A. Chambers, F. Wilhelm, A. Rogalev, Magnetism of Co doped ZnO with Al co-doping: carrier-induced mechanisms versus extrinsic origins, *Phys. Rev. B* 82 (2010) 41202, <https://doi.org/10.1103/PhysRevB.82.041202>.
- [2] J.M.D. Coey, P. Stamenov, R.D. Gunning, M. Venkatesan, K. Paul, Ferromagnetism in defect-ridden oxides and related materials, *New J. Phys.* 12 (2010) 053025, doi:10.1088/1367-2630/12/5/053025.
- [3] A. Ney, A. Kovacs, V. Ney, S. Ye, K. Ollefs, T. Kammermeier, F. Wilhelm, A. Rogalev, R.E. Dunin-Borkowski, Structural, chemical and magnetic properties of secondary phases in Co-doped ZnO, *New J. Phys.* 13 (2011) 103001, <https://doi.org/10.1088/1367-2630/13/10/103001>.
- [4] Q. Huang, Y. Liu, S. Yang, Y. Zhao, X. Zhang, Hydrogen mediated self-textured zinc oxide films for silicon thin film solar cells, *Sol. Energ. Mat. Sol. C.* 103 (2012) 134–139, <https://doi.org/10.1016/j.solmat.2012.03.033>.
- [5] U. Ozgur, Ya.I. Alivov, C. Liu, A. Teke, M.A. Reshchikov, S. Dogan, V. Avrutin, S.J. Cho, H. Morkoc, A comprehensive review of ZnO materials and devices, *J. Appl. Phys.* 98 (2005) 41301, <https://doi.org/10.1063/1.1992666>.
- [6] R.D. Vispute, V. Talyansky, S. Choopun, R.P. Sharma, T. Venkatesan, M. He, X. Tang, J.B. Halpern, M.G. Spencer, Y.X. Li, L.G. Salamanca-Riba, A.A. Iliadis, K.A. Jones, Heteroepitaxy of ZnO on GaN and its implications for fabrication of hybrid optoelectronic devices, *Appl. Phys. Lett.* 73 (1998) 348–350, <https://doi.org/10.1063/1.121830>.
- [7] P. Fons, K. Ivata, S. Niki, A. Yamada, K. Matsubara, Growth of high-quality epitaxial ZnO films on  $\alpha$ -Al<sub>2</sub>O<sub>3</sub>, *J. Cryst. Growth* 201–202 (1999) 627–632, [https://doi.org/10.1016/S0022-0248\(98\)01427-4](https://doi.org/10.1016/S0022-0248(98)01427-4).
- [8] M.A.L. Johnson, S. Fujita, W.H.J. Rowland, W.C. Hughes, J.W. Cook, J.F. Schetzina, MBE growth and properties of ZnO on sapphire and SiC substrates, *J. Electron. Mater.* 25 (1996) 855–862, <https://doi.org/10.1007/BF02666649>.
- [9] Y. Liu, S. Chiu, J.-C.-A. Huang, H. Hsue, Y. Liao, C. Lee, C. Lin, H. Chou, S.F. Chen, C. Liu, Z. Li, H. Qiu, Crystalline effect on ferromagnetism and magneto-transport of epitaxial semiconducting Co:ZnO films, *Thin Solid Films* 605 (2016) 267–272, <https://doi.org/10.1016/j.tsf.2015.10.044>.
- [10] H.-J. Lee, C.H. Park, S.-Y. Jeong, K.-J. Yee, C.R. Cho, M.-H. Jung, D.J. Chadi, Hydrogen-induced ferromagnetism in ZnCoO, *Appl. Phys. Lett.* 88 (2006) 62504, <https://doi.org/10.1063/1.2171789>.
- [11] Y.C. Cho, S.-J. Kim, S. Lee, S.J. Kim, C.R. Cho, H.-H. Nahm, C.H. Park, I.K. Jeong, S. Park, T.E. Hong, S. Kuroda, S.-Y. Jeong, Reversible ferromagnetic spin ordering governed by hydrogen in Co-doped ZnO semiconductor, *Appl. Phys. Lett.* 95 (2009) 172514, <https://doi.org/10.1063/1.3257733>.
- [12] J.H. Park, S. Lee, B.-S. Kim, W.-K. Kim, Y.C. Cho, M.W. Oh, C.R. Cho, S.-Y. Jeong, Effects of Al doping on the magnetic properties of ZnCoO and ZnCoO:H, *Appl. Phys. Lett.* 104 (2014) 52412, <https://doi.org/10.1063/1.4864187>.
- [13] Z.N. Kayani, A. Afzal, E.S. Khan, F. Nazir, F. Saleemi, S.R.S. Naseem, Structural and magnetic properties of CoZnO films, *Materials Today Proc.* 2 (2015) 5473–5476, <https://doi.org/10.1016/j.matpr.2015.11.072>.
- [14] S. Lee, Y.C. Cho, S.-J. Kim, C. Cho, S.-Y. Jeong, S.J. Kim, J.P. Kim, Y.N. Choi, J.M. Sur, Reproducible manipulation of spin ordering in ZnCoO nanocrystals by hydrogen mediation, *Appl. Phys. Lett.* 94 (2009) 212507, <https://doi.org/10.1063/1.3136845>.
- [15] S. Lee, B.-S. Kim, S.-W. Seo, Y.C. Cho, S.K. Kim, J.P. Kim, I.I.-K. Jeong, C.R. Cho, C.U. Jung, H. Koinuma, S.-Y. Jeong, A study of the correlation between hydrogen content and magnetism in ZnCoO, *J. Appl. Phys.* 111 (2012) 07C304, <https://doi.org/10.1063/1.3671786>.
- [16] S. Lee, B.-S. Kim, J.H. Park, T.-W. Lee, Y.C. Cho, S.-Y. Jeong, Study on the formation of magnetic nanoclusters and change in spin ordering in Co-doped ZnO using magnetic susceptibility, *RSC Adv.* 5 (2015) 65840–65846, <https://doi.org/10.1039/c5ra13194d>.
- [17] D.G. Thomas, J.J. Lander, Hydrogen as a donor in zinc oxide, *J. Chem. Phys.* 25 (1956) 1136–1142, <https://doi.org/10.1063/1.1743165>.
- [18] R.K. Singhal, Narendra Jakhar, A. Samariya, S.N. Dolia, Sudhish Kumar, Effect of Co and O defects on ferromagnetism in Co-doped ZnO: an X-ray absorption spectroscopic investigation, *Physica B: Condensed Matter* 530 (2018) 1–6, <https://doi.org/10.1016/j.physb.2017.10.094>.
- [19] M. El-Hilo, A.A. Dakhel, Z.J. Yacoub, Magnetic interactions in Co<sup>2+</sup> doped ZnO synthesized by co-precipitation method: Efficient effect of hydrogenation on the long-range ferromagnetic order, *J. Mag. Mag. Mater* 482 (2019) 125–134, <https://doi.org/10.1016/j.jmmm.2019.03.053>.
- [20] A. Rogalev, F. Wilhelm, J. Goulon, G. Goujon, Magnetism and synchrotron radiation: towards the fourth generation light sources, *Springer Proc. Phys.* 151 (2013) 289–314.
- [21] V. Ney, V. Venkataraman, B. Henne, K. Ollefs, F. Wilhelm, A. Rogalev, A. Ney, Co and Cu co-doped ZnO epitaxial films - a magnetically soft nano-composite, *J. Appl. Phys.* 119 (16) (2016) 163901, <https://doi.org/10.1063/1.4947455>.
- [22] S. Oktik, Low-cost, non-vacuum techniques for the preparation of thin, thick films for photovoltaic applications, *Prog. Cryst. Growth Charact.* 17 (1988) 171–240, [https://doi.org/10.1016/0146-3535\(88\)90006-8](https://doi.org/10.1016/0146-3535(88)90006-8).
- [23] M. Caglar, S. Ilican, Y. Caglar, F. Yakuphanoglu, Electrical conductivity and optical properties of ZnO nanostructured thin film, *Appl. Surf. Sci.* 255 (2009) 4491–4496, <https://doi.org/10.1016/j.apsusc.2008.11.055>.
- [24] K. Ando, H. Saito, Z. Jin, T. Fukumura, M. Kawasaki, Y. Matsumoto, H. Koinuma, Magneto-optical properties of ZnO-based diluted magnetic semiconductors, *J. Appl. Phys.* 89 (2001) 7284–7286, <https://doi.org/10.1063/1.1356035>.
- [25] W.H. Breckenridge, J.-H. Wang, Dynamics of the reactions of Zn(4s4p <sup>3</sup>P<sub>1</sub>) with H<sub>2</sub>,

- HD, and D<sub>2</sub>: Rotational and vibrational quantum-state distributions of ZnH (ZnD) products, *J. Chem. Phys.* 87 (1987) 2630–2637, <https://doi.org/10.1063/1.453101>.
- [26] K.Yu. Zhizhin, N.N. Mal'tseva, G.A. Buzanov, N.T. Kuznetsov, Hydride compounds of zinc, *Russian J. Inorg. Chem.* 59 (2014) 1665–1678, <https://doi.org/10.1134/S003602361414006X>.
- [27] A. Shayesteh, D.R.T. Appadoo, I.E. Gordon, P.F. Bernath, Vibration-rotation emission spectra of gaseous ZnH<sub>2</sub> and ZnD<sub>2</sub>, *J. Am. Chem. Soc.* 126 (2004) 14356–14357, <https://doi.org/10.1021/ja046050b>.
- [28] H. Saeki, H. Matsui, T. Kawai, H. Tabata, Transparent magnetic semiconductors based on ZnO, *J. Phys.: Condens. Matter* 16 (2004) S5533–S5540, <https://doi.org/10.1088/0953-8984/16/48/008>.
- [29] K. Ando, H. Saito, V. Zayets, M.C. Debnath, Optical properties and functions of dilute magnetic semiconductors, *J. Phys.: Condens. Matter* 16 (2004) S5541–S5548, <https://doi.org/10.1088/0953-8984/16/48/009>.
- [30] W.K. Liu, G.M. Salley, D.R. Gamelin, Spectroscopy of photovoltaic and photoconductive nanocrystalline Co<sup>2+</sup>-doped ZnO electrodes, *J. Phys. Chem. B* 109 (2005) 14486–14495, <https://doi.org/10.1021/jp0518781>.
- [31] K.R. Kittilstved, J. Zhao, W.K. Liu, J.D. Bryan, D.A. Schwartz, D.R. Gamelina, Magnetic circular dichroism of ferromagnetic Co<sup>2+</sup>-doped ZnO, *Appl. Phys. Lett.* 89 (2006) 62510, <https://doi.org/10.1063/1.2221871>.
- [32] J.R. Neal, A.J. Behan, R.M. Ibrahim, H.J. Blythe, M. Ziese, A.M. Fox, G.A. Gehring, Room temperature magneto-optics of ferromagnetic transition-metal doped ZnO thin films, *Phys. Rev. Lett.* 96 (2006) 197208, <https://doi.org/10.1103/PhysRevLett.96.197208>.
- [33] Y. Fukuma, F. Odawara, H. Asada, T. Koyanagi, Effects of annealing and chemical doping on magnetic properties in Co-doped ZnO films, *Phys. Rev. B* 78 (2008) 104417, <https://doi.org/10.1103/PhysRevB.78.104417>.
- [34] S. Deka, P.A. Joy, Ferromagnetism induced by hydrogen in polycrystalline non-magnetic Zn<sub>0.95</sub>Co<sub>0.05</sub>O, *Appl. Phys. Lett.* 89 (2006) 32508, <https://doi.org/10.1063/1.2227642>.
- [35] Y. Fukuma, H. Asada, J. Yamamoto, F. Odawara, T. Koyanagi, Large magnetic circular dichroism of Co clusters in Co-doped ZnO, *Appl. Phys. Lett.* 93 (2008) 142510, <https://doi.org/10.1063/1.2992631>.
- [36] S.J. Kim, S.Y. Cha, J.Y. Kim, J.M. Shin, Y.C. Cho, S. Lee, W.-K. Kim, S.-Y. Jeong, Y.S. Yang, C.R. Cho, H.W. Choi, M.-H. Jung, B.-E. Jun, K.-Y. Kwon, Y. Kuroiwa, C. Moriyoshi, Ferromagnetism in ZnCoO due to hydrogen-mediated Co–H–Co complexes: how to avoid the formation of Co metal clusters? *J. Phys. Chem. C* 116 (2012) 2196–2202, <https://doi.org/10.1021/jp300536w>.
- [37] M. Yu, H. Qiu, X. Chen, H. Liu, Magnetic, magnetoresistance and electrical transport properties of Ni and Al co-doped ZnO films grown on glass substrates by direct current magnetron co-sputtering, *Mater. Chem. Phys.* 120 (2010) 571–575, <https://doi.org/10.1016/j.matchemphys.2009.12.007>.
- [38] I.S. Edelman, O.V. Vorotynova, V.A. Seredkin, V.N. Zabluda, R.D. Ivantsov, Y.I. Gatiyatova, V.F. Valeev, R.I. Khabullin, A.L. Stepanov, Magnetic and magneto-optical properties of ion-synthesized cobalt nanoparticles in silicon oxide, *Phys. Sol. St.* 50 (2008) 2088–2094, <https://doi.org/10.1134/S1063783408110140>.
- [39] D.A. Petrov, I.S. Edelman, R.D. Ivantsov, S.M. Zharkov, A.L. Stepanov, Magneto-optics of cobalt and nickel nanoparticles implanted in SiO<sub>2</sub>: comparative study, *Sol. St. Phen.* 215 (2014) 214–217, <https://doi.org/10.4028/www.scientific.net/SSP.215.214>.